Innovative experimental setup for thermal and electrical characterization of silicon solar cells under controlled environmental conditions

Benoit Guillo Lohan[a,b,*], Mohamed Amara[a,b,*], Anne Kaminski-Cachopo[c], Mustapha Lemiti[b]

[a] Univ. Lyon, CNRS, INSA-Lyon, Université Claude Bernard Lyon 1, CETHIL UMR5008, F-69621 Villeurbanne, France
[b] Univ. Lyon, CNRS, INSA-Lyon, Université Claude Bernard Lyon 1, INL UMR5270, F-69621 Villeurbanne, France
[c] Univ. Grenoble Alpes, CNRS, Grenoble INP, IMEP-LAHC, F-38000 Grenoble, France

A B S T R A C T

The optimization of solar cells properties with thermal criteria gives the possibility to achieve higher conversion efficiency in outdoor conditions. An innovative setup that allows the control of the surroundings of a solar cell is described. Under such specific conditions, the cell temperature can be stabilized and measured. The variation of the cell temperature with the applied bias is experimentally observed and quantified. Between short circuit current density (J_{sc}) and open circuit voltage (V_{oc}), a slight difference of temperature is observed, revealing a variation of the thermal equilibrium between these two points. The resistivity of the absorber and the input power density are found to influence this temperature shift. From the experimental results, it appears that the emissivity of the solar cell increases with the applied voltage due to an increase in the excess carrier concentration. Consequently, the operating temperature at open-circuit is lower than at short-circuit.

1. Introduction

One of the biggest challenges for solar cells is to increase their electrical performance. For silicon solar cells, 26.7% conversion efficiency [1] has been recently achieved. This record was obtained under standard test conditions (STC), meaning that the cell temperature was fixed to 25 °C under a specific irradiance of 1000 W m^{-2} (1 sun) with AM1.5G spectrum. However, these conditions do not reflect the real functioning conditions. The cell is, in fact, exposed to much higher temperature, which degrades its conversion efficiency. In 1981, D.L Evans observed that the solar cell efficiency at a temperature T can be linked to its efficiency at a reference temperature T_{ref}, by defining the temperature degradation coefficient β (in °C^{-1}) [2]:

$$\eta(T) = \eta(T_{ref}) \cdot (1 - \beta \cdot (T - T_{ref})) \qquad (1)$$

The β coefficient depends on the device characteristics, the architecture but also the environmental conditions [3–5]. As a result, a way to improve the global solar cell conversion efficiency in outdoor conditions could be to optimize, with thermal criteria, their electrical properties and fabrication process. A better understanding of the electrical and thermal behavior (ETB) of solar cells is therefore crucial, as it has been recently shown by Weiss et al. [6]. Despite its significance, the

effect of temperature on solar cell conversion efficiency is sparsely studied in the literature. There are few studies which are analyzing the behavior of solar modules in outdoor conditions. For example, Almonacid et al. [7] are relating the cell temperature variations with meteorological parameters, while Kamkird et al. [8] and Vogt et al. [9] are comparing the thermal behavior of different solar cell modules in outdoor conditions. However, none of these experimental studies allow the separation of each environmental effect on the ETB of solar cells. In this work, we present an innovative experimental setup giving the possibility to measure the cell temperature under controlled environmental conditions. Unlike the existing characterization setups usually presented in the literature, the cell temperature is not imposed by conduction at the bottom of the cell [10] but by radiative exchanges, offering more possibilities for the study of the ETB of solar cells.

This paper starts with the description of the physical phenomenon involved in the thermal equilibrium between a solar cell and its environment. Then, the innovative experimental setup developed in-house is presented. Afterwards, the evolution of the cell temperature with the applied bias is studied, and compared to numerical simulations. Finally, the influence of the base resistivity of the absorber and the light intensity on the solar cell ETB is investigated.

* Corresponding authors at: Univ. Lyon, CNRS, INSA-Lyon, Université Claude Bernard Lyon 1, INL UMR5270, F-69621 Villeurbanne, France.
  E-mail address: Mohamed.Amara@insa-lyon.fr (M. Amara).

2. Preliminary study: modelling of solar cells ETB

2.1. General approach: influence of the temperature on IV characteristic

The influence of the temperature on solar cell electrical characteristics has already been explored in literature: the increase of the cell temperature leads to a deterioration of its electrical efficiency. When increasing the cell temperature, on the I-V curve the consequences are the following:

- A slight increase of the short-circuit current density (J_{sc}),
- A drop of the open-circuit voltage (V_{oc}).

These variations are related to different properties of the solar cell. For most semiconductors, including silicon, higher temperatures tend to reduce the band gap of the materials [11]. More photons will have enough energy to be absorbed [12], resulting in higher short circuit current density. However, the amplification of the diode current, caused by the increase of intrinsic carrier concentration, tends to dramatically decrease the open circuit voltage [13,14]. This drop of V_{oc}, when increasing the temperature, is mainly responsible for the loss of conversion efficiency of the solar cell under operating conditions [15].

The aim of this article is to analyze the different mechanisms involved in the thermal equilibrium between a solar cell and its environment under operating conditions. This study will be used to estimate the operating temperature of the solar cell for specific environmental conditions.

2.2. Modelling the ETB of silicon solar cells: effect of the applied bias

Under illumination, a solar cell will reach an operating temperature, which not only depends on the environmental conditions but also on its properties such as the base doping or the considered architecture. The Nominal Operating Cell Temperature (NOCT) is measured under specific conditions: an input power density of 800 W/m^{-2}, an ambient temperature of 25 °C and a given wind speed of 1 m·s^{-1}. This temperature is measured at V_{oc} and is supposed to stay constant whatever the applied bias. A simple power exchange analysis can be performed to invalidate this assumption. As the electrical power which can be extracted from the cell culminates at maximum power point M_{pp}, the contribution of the incident solar power to the thermal heating of the cell decreases when approaching M_{pp}. Consequently, the cell temperature at M_{pp} is lower than the ones at V_{oc} and J_{sc}. A complete study of the different heating and cooling mechanisms involved in the thermal equilibrium between a solar cell and its environment is necessary to quantify this variation of temperature with the applied bias.

This study was performed in a previous paper [16], in which the ETB of a solar cell under specific environmental conditions was simulated by coupling radiative transfer, heat transfer and transport equations. For a given applied bias and boundary conditions, the electrical output power and the cell temperature are calculated for a solar cell with the parameters defined in Table 1. The heat transfer convective coefficient between the cell and the surrounding was set to 1 W·m^{-2}·K^{-1} (this coefficient cannot be null because of convergence issues). The

Table 1
Parameters of the simulated solar cell.

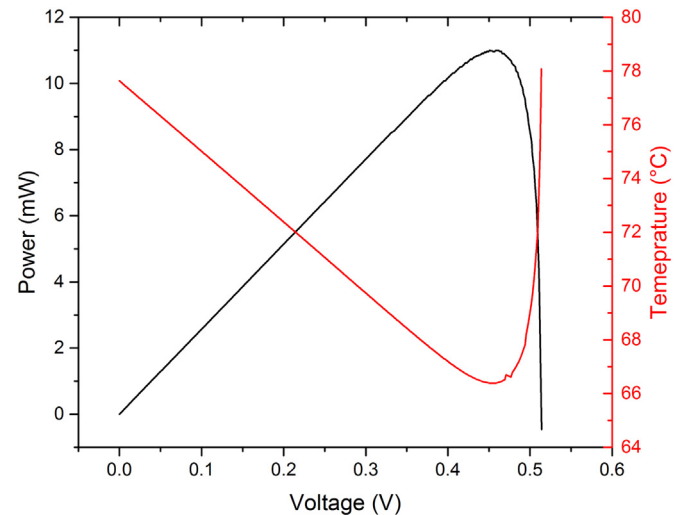| Parameter	Value
Wafer thickness	275 μm
Base Doping (p-type, uniform)	1×10^{16} cm^{-3}
Emitter Doping (n-type, uniform)	5×10^{19} cm^{-3}
Junction Depth	300 nm
Front surface recombination velocity	1000 cm·s^{-1}
Rear surface recombination velocity	10000 cm·s^{-1}
SRH Lifetime	1 ms

Fig. 1. Power and temperature-voltage characteristics of the simulated solar cell.

numerical model does not include surface texturation, shunt resistance is supposed infinite and series resistance null. The recombination at the interface between the semiconductor and the metal are also neglected. Besides, low injection is assumed for the transport equations calculation.

The results presented on Fig. 1 confirm the simple analysis presented in the previous study. For the given solar cell parameter, we observe the following points: the cell reaches a maximum temperature value at J_{sc} and V_{oc} (78 °C), and a minimum value at M_{pp} (66.5 °C). The numerical model gives the possibility to quantify the cell temperature variation between J_{sc}, V_{oc} and M_{pp}. Moreover, we will see in the section "Results and Discussion" that the temperature at V_{oc} may differ from the one at J_{sc}.

For three specific points (J_{sc}, M_{pp} and V_{oc}), the different heating and cooling mechanisms involved in the thermal equilibrium between the cell and its environment were fully explored in a previous investigation [16]. These mechanisms are either responsible for the heating of the cell (Joule effect, Peltier effect, recombination process or thermalization) or for its cooling (Thermal radiation, convective exchange or Thomson effect).

Due to the thermal equilibrium between heating and cooling mechanisms, the temperature of the cell can be stabilized for each applied bias. The variation of heat sources and sinks explains the cell temperature variation presented in Fig. 1 [16].

With the use of the numerical model, we have highlighted the influence of the applied bias on the ETB of unencapsulated silicon solar cells.

By limiting the different heat and sink sources, such variation of the cell temperature with the applied bias could be measured and quantified. For these reasons, an innovative experimental setup allowing the electro-thermal characterizations of silicon solar cells under controlled environmental conditions is introduced.

3. Development of an innovative experimental setup

3.1. Presentation of the experimental setup

In this paragraph, we present a setup which allows a control of the surroundings of a solar cell. At the same time, the electrical performances of the solar cell are measured. To ensure such measurement, the setup must have the following features:

- Control of the different thermal exchanges between the cell and the surroundings (including radiation, convection and conduction),
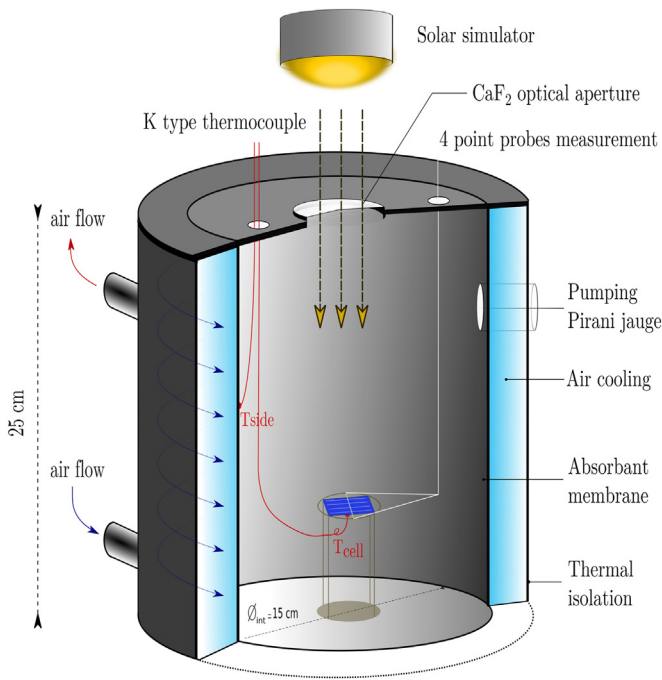
Fig. 2. Innovative experimental setup for ETB study of silicon-based solar cells.

- Measurement of the cell temperature and its P-V characteristic.

The setup was designed, dimensioned and set in order to control each external parameter which plays a role in determining the operating temperature of a solar cell (Fig. 2). The sample is placed in a cylindrical chamber (15 cm diameter and 25 cm height), where the inner side is fully covered by an absorbent membrane with a very high emissivity. As a result, the inner side will behave like a black body at a specific temperature. The inner side temperature of the enclosure is controlled using an air-cooling system within a range from 5 °C to 50 °C, allowing the simulation of extreme outside conditions. The enclosure is thermally isolated from the outside to avoid the influence of external parameters such as the room temperature. A pumping system allows the work under vacuum, reaching 0.3 mbar. As the convective exchanges cannot easily be controlled, the work under vacuum is necessary if we want to compare the ETB of different solar cells. To observe the influence of the convective exchanges, we plotted for different inner pressure (5 mbar, 0.5 mbar and 0.1 mbar) the evolution of the cell temperature against time. The same cell temperature was measured in each experiment, which leads us to the conclusion that the convective exchanges can be neglected compare the radiative ones. Moreover, at this pressure, the conductive exchange with the air can be neglected. The cell is held by its four corners as presented in Fig. 3, limiting therefore the conduction losses. As a result, the radiative exchanges between the cell and its surroundings will be responsible for the thermal equilibrium
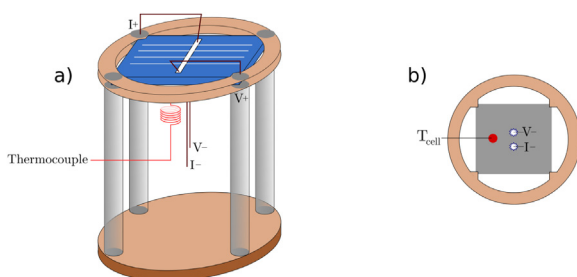

Fig. 3. Schematic views of the sample holder, where the cell is held by its four corners: a) lateral view and b) back-side view.

observed with the developed experimental setup.

One should notice that only the sides of the enclosure are cooled by the air-flow. By considering the radiative exchange between the cell and each part of the enclosure, we assumed that the temperature variation of the cover and the bottom, have almost no influence on the cell temperature. This hypothesis was confirmed using view factor calculation. A 40 mm diameter calcium fluoride (CaF_2) optical aperture separates the housing from the outside. A xenon arc lamp (1 sun, AM1.5G) was used as a light source. Regarding the spectrum validity, the absolute irradiance was measured with a spectrometer (FLAME-S Silicon detector), and compared to AAA class xenon arc lamp spectrum. The results are in good agreement with the reference solar spectral irradiance (ASTM G-173). The input electrical power of the arc lamp and the position of the sample were calibrated using a reference cell (FHG RS-ID-4) with given specifications. I-V characteristics are obtained with a Keithley sourcemeter using the four points probe mode. Standardized K-type thermocouples ensure the temperature measurement of the cover, the inner side, the atmosphere and the sample. The thermocouple used for the cell temperature measurement is mounted on a spring (Fig. 3), meaning that the presented characterization is a non-destructive method. Such measurement method is possible because the cell is placed under the primary vacuum. Considering the thermal conductivity of the silicon, the temperature measured on the back side of the sample is assumed to be the cell temperature.

Under illumination and under low pressure (0.3 mbar), we are able to measure the cell operating temperature for stabilized environmental conditions. Both 1 cm² and 4 cm² solar cells can be placed in the cylindrical chamber. However, we chose to work on 1 cm² p-type silicon solar cells, fabricated in-house, because higher input power density can be reached with smaller solar cells. The different samples used are listed:

- Passivated Emitter Rear Totally diffused (PERT)
- Passivated Emitter and Rear Cells (PERC)
- Aluminum Back Surface Field (Al-BSF) cells

3.2. Measurement protocol: cell temperature stabilization under given experimental conditions

To illustrate the measurement protocol, a 1 cm² p-type ($\rho \sim 5.5$ $\Omega \cdot cm$) p-PERC silicon solar cell was used. Placed under illumination, and for an inner temperature of 25 °C, the solar cell is reaching a temperature of 51 °C. This thermal equilibrium was obtained at J_{sc}, meaning that no bias was applied to the cell.

Once the thermal equilibrium is reached, electrical plateaux from V_{oc} to J_{sc} (Fig. 4) were applied. For each electrical plateau, the evolution of the cell temperature and the output electrical power were measured. In steady state conditions, when the cell temperature is stabilized, we are able to measure the couple (Voltage, Electrical Power, Cell temperature).

All the experimental data presented in this work were carried out using the same experimental protocol as described in this paragraph, featuring an inner temperature of 25 °C and a pressure of 0.3 mbar. However, it should be emphasized that these conditions do not correspond to the real operating conditions.

4. Results and discussion

4.1. Evolution of the cell temperature with the applied bias

Using the characterization methodology described above, we are able to simultaneously plot the evolution of the cell temperature and the electrical output power versus the applied bias after the temperature stabilization at 51 °C. For uncertainty quantification, the same experiment was performed three times in a row on the same solar cell, under rigorously identical conditions (pressure and temperature of the
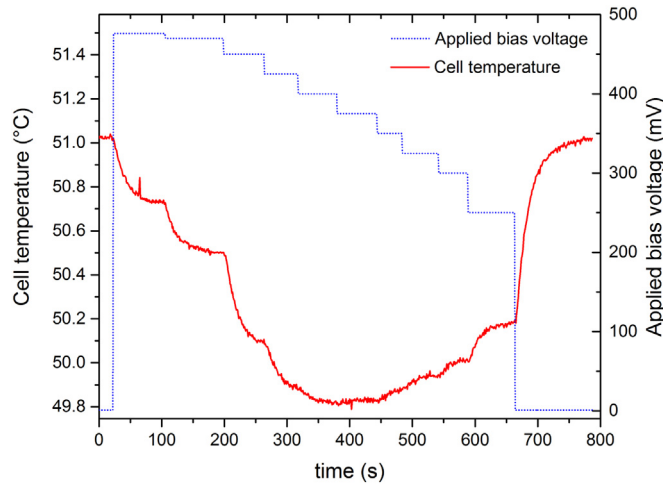
Fig. 4. Evolution of the cell temperature versus time for different applied bias.
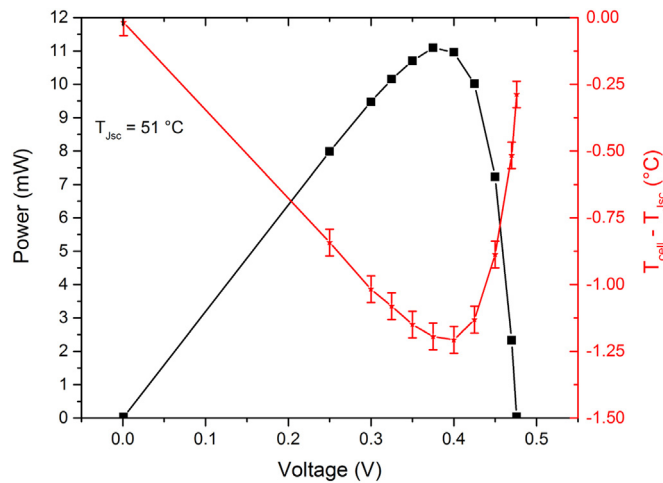

Fig. 5. Influence of the applied bias on the electrical output power (dark curve) and on the cell temperature (red curve) for a p-PERC solar cell with a base resistivity of $\rho \sim 5.5\,\Omega \cdot cm$.

inner side). For the p-PERC solar cell, the results are presented in Fig. 5. The red curve shows the cell temperature variation compared to its value at J_{sc} while the black one gives the electrical output power for each applied bias. As expected, the cell temperature is varying with the applied bias, reaching a minimum value for a given applied voltage and a maximum value at J_{sc}. No hysteresis on the cell temperature measurement was observed between forward and reverse bias.

This variation agrees with some aspects of the simulation (Fig. 1). The temperature dependence with the applied bias induces a decrease of the cell temperature of 1.5 °C from J_{sc} to M_{pp}. Due to the very high sensitivity of the electrical efficiency with the temperature, an increase of $+0.1\%$ abs. of the electrical efficiency is observed compared to the case where the temperature is supposed to be constant along the characterization.

However, some discrepancies between the experimental results and the numerical simulations have to be underlined. In fact, the following points were observed:

- The measured temperature at J_{sc} is lower than the one obtained by simulation.
- The temperature at V_{oc} is lower than the one at J_{sc}.
- The minimum temperature does not correspond to M_{pp}.
- The variation of temperature $\Delta(T_{max}-T_{min})$ is much lower than the one expected by the numerical model ($+1.25$ °C for the

experimental against $+11.5$ °C for the numerical).

Regarding the disparities presented above, we argue that the discrepancies between numerical and experimental results might be partly due to the following points: *I)* The thermal emission of the cell is calculated regardless of minority carriers concentration. *II)* The model simulates a single p-n junction, without taking into account the influence of the BSF [17] *III)* The p-n junction is modeled using the depletion approximation: the electrical field only appears in the space charge region [16] meaning that the total joule heat source is only calculated in the space charge region (SCR) *IV)* The numerical model is 1D, where the lateral movement of carriers are not taken into account, especially in the emitter region *V)* Low injection is assumed; the total current density is obtained by solving the transport equations of minority carriers in the quasi-neutral regions added to the current density in the SCR *VI)* The numerical model simulates flat solar cell. The emissivity of the cell strongly increases with texturization [18].

Nevertheless, despite these discrepancies, the numerical and experimental results were found to have the same trends.

Focus is now set on the cell temperature variation between J_{sc} and V_{oc}. With the presented methodology, a precise analysis of the influence of different parameters (such as the base resistivity or light intensity) on the ETB of the solar cell was performed, using the in-house fabricating solar cells.

4.2. Temperature variation between J_{sc} and V_{oc}

4.2.1. Effect of the base resistivity

For a p-PERC solar cell with a base resistivity close to $1\,\Omega \cdot cm$, the evolution of its temperature and electrical output power versus the applied bias are presented in Fig. 6 and compared to the one obtained for the p-PERC cell with a base resistivity of $5.5\,\Omega \cdot cm$. It appears that, when decreasing the resistivity (which corresponds to an increase of the base doping), the difference of temperature between J_{sc} and V_{oc} is also decreasing. For lower base resistivity, higher temperature variation between J_{sc} and M_{pp} can be observed. It should be pointed out that a decrease of the base doping leads to a decrease of the V_{oc} [19], which partly explain the low V_{oc} of the $5.5\,\Omega \cdot cm$ cell compared to the $1\,\Omega \cdot cm$ one.

To confirm the influence of the base resistivity, experiments on different solar cell structures and base resistivity (between 1 and 6.6 $\Omega \cdot cm$) were carried out. All electrical efficiency values at 25 °C are
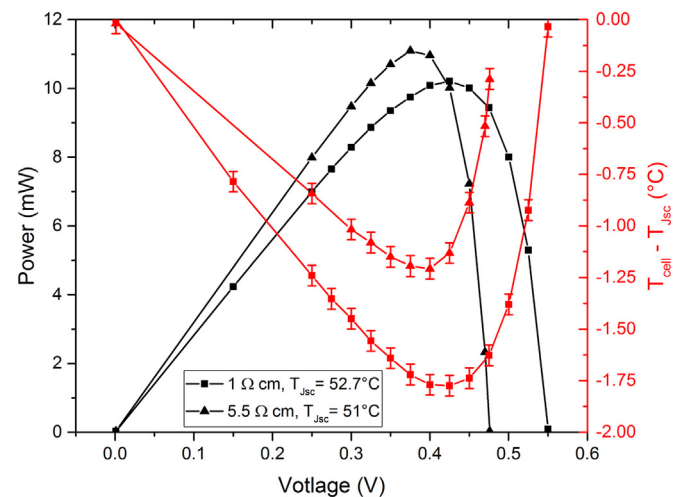

Fig. 6. Evolution of the electrical output power (dark curves, solid lines) and cell temperature (red, dashed lines) with the applied bias for a p-PERC solar cell with a base resistivity of $\sim 1\,\Omega \cdot cm$ and a p-PERC solar cell with a base resistivity of $5.5\,\Omega \cdot cm$.

Table 2
Evolution of T_{Jsc}-T_{Voc} for solar cells with different base resistivity.

Sample name	Base Resistivity ($\Omega \cdot cm$)	η (%) (@25 °C)	T_{Jsc} (°C)	$T_{Jsc} - T_{Voc}$ (°C)
PERT#1	~ 6.8	14.6	53.08 ± 0.05	0.80 ± 0.05
PERT#2	~ 6.8	15.2	54.37 ± 0.05	0.82 ± 0.05
Al-BSF#1	~ 1.9	15.41	52.57 ± 0.05	0.43 ± 0.05
Al-BSF#2	~ 2.2	15.92	52.89 ± 0.05	0.56 ± 0.05
poly-Al-BSF#1	~ 1	12.35	54.21 ± 0.05	0.00 ± 0.05
poly-Al-BSF#2	~ 1	11.95	52.69 ± 0.05	0.00 ± 0.05
PERC#1	~ 5.5	15.45	50.58 ± 0.05	0.28 ± 0.05
PERC#2	~ 6.1	15.81	50.72 ± 0.05	0.38 ± 0.05
PERC#3	~ 5.3	15.83	51.12 ± 0.05	0.19 ± 0.05
PERC#4	~ 1	16.1	52.15 ± 0.05	0.00 ± 0.05

included within the range 14.6–16.1% (except for poly-AlBSF cells with efficiency closed to 12%. The base resistivity was measured on the wafer before the fabrication process.

Looking at the results presented in Table 2, it seems that both resistivity and cell architecture influence the variation Δ(T_{Jsc}-T_{Voc}). These results are also presented in Fig. 7 where the evolution of T_{Jsc}-T_{Voc} for the different sample is plotted. Regarding the experimental values, a general trend can be observed: increasing the base resistivity of a solar cell leads to an increase of the temperature variation between J_{sc} and V_{oc}. It should be emphasized that under identical environmental conditions, PERC setup reaching lower operating temperature value than Al-BSF cells (see Table 2), which is consistent with the recent results presented by Vogt et al. [9].

4.2.2. Effect of the input power density

With the installation of a Fresnel lens, different input power densities can be reached, from around 0.5 sun to 3 suns. For these lower and upper limit, electro-thermal characterizations were carried out on a solar cell with a base resistivity of 6.6 $\Omega \cdot cm$, under identical environmental conditions. Fig. 8 presents the variation of the cell temperature compared to its value at J_{sc} and the electrical output power for two input power densities: 0.5 and 3 suns. When increasing the light intensity, the cell is reaching higher temperature stabilization at J_{sc} (41 °C for 0.5 sun against 73.5 °C for 3 suns). Moreover, the expected drop of open circuit voltage due to the increase of temperature is compensated by its dependence on the short circuit current density because of the increase of input power density Fig. 9.

Concerning the difference of temperature between J_{sc} and V_{oc} at 0.5 sun, it is small under 0.5 sun (less than 0.1 °C) whereas it dramatically
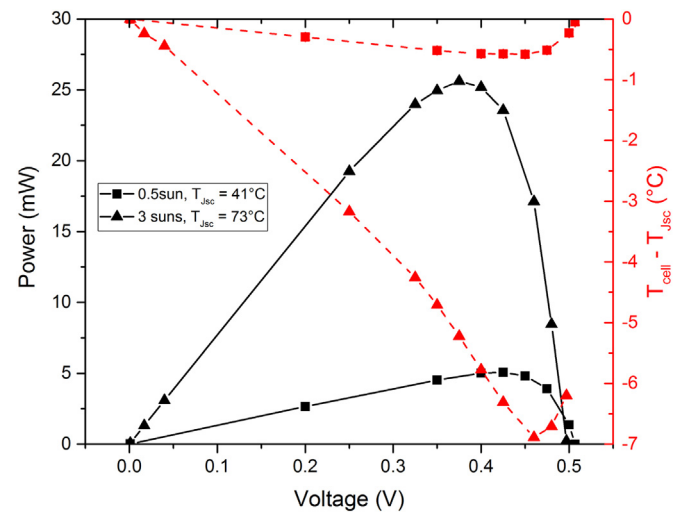

Fig. 8. Influence of light intensity on the ETB of a silicon solar cell with a base resistivity of 6.6 $\Omega \cdot cm$.

increases under 3 suns (> 6 °C for 3 suns). One should also notice that the minimum cell temperature is shifting to V_{oc} when increasing the light intensity and does not correspond to the maximum power point.

4.3. Discussions

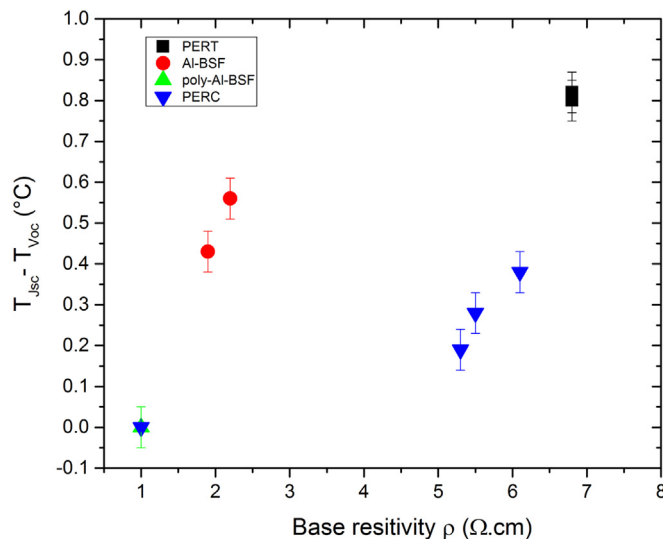From the obtained results, both base resistivity and light intensity

Fig. 7. Influence of the base resistivity of solar cells on the variation T_{Jsc}-T_{Voc}.
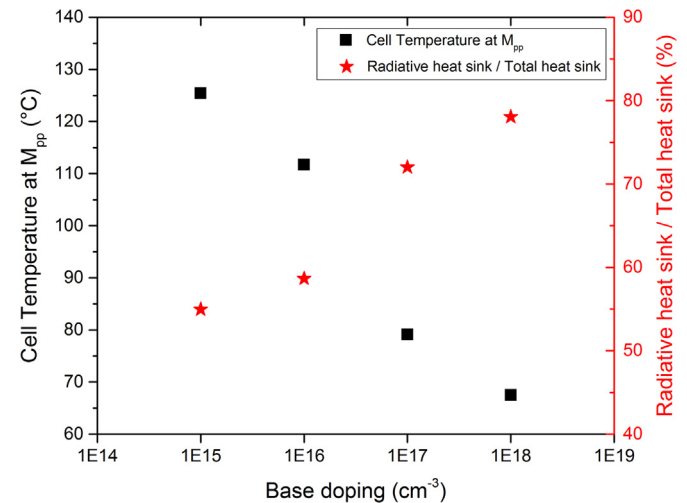

Fig. 9. Evolution of the cell operating temperature at M_{pp} with the base doping. The evolution of the radiative heat sink compared to the total cooling source is also presented.

influence the temperature variation between V_{oc} and J_{sc}. Kirschoff's law links the thermal emission and absorption coefficient at the wavelength λ for a given direction $\vec{r}$:

$$\alpha_\lambda(\vec{r}) = \epsilon_\lambda(\vec{r}) \qquad (2)$$

Under thermal equilibrium conditions, the absorption coefficient of the cell is ruling its thermal emission and depends on the lattice absorption and the free carrier absorption as:

$$\alpha = \alpha_{lattice} + \alpha_{FCA} \qquad (3)$$

The free carrier concentration, assumed to be ruled by majority carriers concentration under low injection hypothesis, is a key parameter for the calculation of the absorption coefficient. Usually, the free carrier absorption coefficient is defined as a function of the wavelength λ and N the concentration of free carrier, such as [20]:

$$\alpha_{FCA} = C \cdot N \cdot \lambda^\gamma \qquad (4)$$

where C is a constant and γ varies from 1.5 to 3.5, expressing the evolution of scattering mechanisms with energy [20]. As a result (4) shows that the radiative cooling of the cell can be enhanced by increasing the free carriers concentration. Such enhancement can be performed by changing the base doping. Using the numerical model, we are able to simultaneously plot the evolution of the cell temperature and the evolution of the radiative cooling contribution compared to the total heat sink, at M_{pp}, for different base doping (from 1×10^{15} cm^{-3} to 1×10^{18} cm^{-3}) with low convective exchanges.

We observed that the cell operating temperature at M_{pp} decreases when increasing the base doping because of the increase of the majority carriers concentration, which underlines the contribution of free carriers to the thermal emissivity of the cell.

In the solar cell structure, two parts have to be distinguished: the emitter and the base. Because the emitter is usually highly doped, the contribution of minority carriers (holes for a n-doped emitter) to the free carrier concentration in this region can be neglected. However, in the absorber, the resistivity is usually close to $1.5\,\Omega\cdot$cm, corresponding to a dopant concentration (N_D) around 9.7×10^{15} cm^{-3}. For a p-type solar cell under direct bias, the electrons concentration in the base is defined as:

$$n = n_0 + \Delta n_{inj}(ph) + \Delta n_{inj}(V) \qquad (5)$$

Where n_0 is the equilibrium electron density, $\Delta n_{inj}(ph)$ the contribution of photogenerated carriers due to incoming light and $\Delta n_{inj}(V)$ the contribution of electrons injected by polarization from n-region to p-region.

$\Delta n_{inj}(V)$ increases with the applied bias and reaches its maximal value at V_{oc}. From this analysis, the free carriers concentration N defined by (4) is higher at V_{oc} than the one at J_{sc}, which leads to an increase of the absorption coefficient defined by (3) with the applied bias. As a result, $T_{Jsc} > T_{Voc}$.

When increasing the base resistivity, the majority carriers concentration is decreasing. Besides, at J_{sc}, the minority carriers concentration is lower by several orders of magnitude than the majority one. However, as minority carriers concentration is increasing with the applied bias, the ratio between minority and majority carriers concentrations is also increasing when approaching the open circuit voltage. Using PC1D numerical simulation for a 2.3×10^{15} cm^{-3} p-doped solar cell ($\sim 6\,\Omega\cdot$cm), the minority carriers concentration goes from 1×10^{13} cm^{-3} at J_{sc} to 1.82×10^{15} cm^{-3} at V_{oc}.

The higher the base resistivity, the higher the variation of the free carriers concentration N between J_{sc} and V_{oc}, because of a greater influence of minority carriers on α_{FCA}. As a result, $\Delta(T_{Jsc}-T_{Voc})$ increases when increasing the base resistivity. When increasing the input power density, the minority carriers concentration increases significantly, and so their contribution to the thermal exchange by radiation.

We also observed that for a $1\,\Omega\cdot$cm p-PERC solar cell, the variation $\Delta(T_{Jsc}-T_{Voc})$ went from 0 °C under 1 sun to 0.25 °C under 3 suns. This small difference is explained by the fact that, as the base is highly doped, the increase of minority carriers concentration due to the incoming light will not be sufficient enough to observe a distinct variation of temperature between J_{sc} and V_{oc}, which is consistent with our statement.

With these discussions, it comes that the difference of temperature between V_{oc} and J_{sc} is increasing with the resistivity of the absorber and the input power density.

5. Conclusion and outlook

In this paper, we have presented an innovative experimental setup allowing the study of the ETB of silicon-based-solar cells under controlled experimental conditions.

The evolution of the cell temperature with the applied bias and its consequences on the electrical behavior of a silicon solar cell was simulated during a previous investigation [16]. With an in-house developed setup, the ETB of silicon solar cells was observed and quantified for the first time, highlighting some discrepancies between numerical and experimental results. Nevertheless, identical trends were observed regarding the variation of the cell temperature with the applied bias. Thanks to the obtained results, the numerical model will be enhanced aiming a better fit of the experimental results.

The experimental results were obtained under specific conditions, where the radiative exchanges between the cell and its surroundings are mainly responsible for the thermal equilibrium reached in the chamber. However, these conditions do not reflect the real operating conditions, where the solar cell is encapsulated, and the convective and conductive exchanges are not minimized. In fact, for an encapsulated solar cell, the glass and the EVA will modify the emissivity of the cell, which may result in an increase of the effective heat coefficient ($h_{rad} + h_{conv}$). In a previous work [21], it has been shown that even for a high heat transfer convective coefficient value, a variation of $\Delta T(V)$ can still be observed. As a result, we believe that for an encapsulated module under real conditions, a variation of the temperature with the applied bias could still be measured. Such study could be the purpose of a future work.

Through this work, the temperature difference between J_{sc} and V_{oc} has also been investigated. For a lightly doped material, the contribution of minority carriers in the bulk region fosters the thermal exchange by radiation between the cell and its environment. As the minority carriers density increases with the applied bias, it appears that the temperature at V_{oc} is lower than the one at J_{sc}, which comes from an increase of the solar cell emissivity with the applied bias. Such study is of great importance, as solar cell emissivity calculations are gaining interest in the PV community [17].

Further studies will focus on the influence of other solar cell parameters on temperature difference between J_{sc} and M_{pp} in order to optimize, with thermal criteria, electrical properties. The effect of base doping on the cell operating temperature should also be investigated. A complete comparative study on the ETB of solar cells under concentration is also necessary, as the optimization of solar cells properties with thermal criteria is a new effective way to achieve higher conversion efficiency under real operating conditions [22].

Acknowledgement

References

[1] M.A. Green, Y. Hishikawa, W. Warta, E.D. Dunlop, D.H. Levi, J. Hohl-Ebinger,

A.W. Ho-Baillie, Solar cell efficiency tables (version 50), Prog. Photovolt. Res. Appl. 25 (7) (2017) 668–676.

[2] D.L. Evans, Simplified method for predicting photovoltaic array output, Sol. Energy 27 (6) (1981) 555–560.

[3] A. Virtuani, D. Pavanello, G. Friesen, Overview of temperature coefficients of different thin film photovoltaic technologies, in: Proceedings of the 25th European photovoltaic solar energy conference and exhibition/5th World conference on photovoltaic energy conversion, 2010, pp. 6–10.

[4] E. Skoplaki, J.A. Palyvos, Operating temperature of photovoltaic modules: A survey of pertinent correlations, Renew. Energy 34 (1) (2009) 23–29.

[5] H. Steinkemper, I. Geisemeyer, M.C. Schubert, W. Warta, S.W. Glunz, Temperature-dependent modeling of silicon solar cells–eg, n i, recombination, and VOC, IEEE J. Photovolt. 7 (2) (2017-03) 450–457.

[6] L. Weiss, M. Amara, C. Ménézo, Impact of radiative-heat transfer on photovoltaic module temperature, Prog. Photovolt: Res. Appl. 24 (1) (2016) 12–27.

[7] F. Almonacid, P.J. Pérez-Higueras, E.F. Fernández, P. Rodrigo, Relation between the cell temperature of a HCPV module and atmospheric parameters, Sol. Energy Mater. Sol. Cells 105 (2012) 322–327.

[8] P. Kamkird, N. Ketjoy, W. Rakwichian, S. Sukchai, Investigation on temperature coefficients of three types photovoltaic module technologies under thailand operating condition, Procedia Eng. 32 (2012) 376–383.

[9] M.R. Vogt, H. Schulte-Huxel, M. Offer, S. Blankemeyer, R. Witteck, M. Kontges, K. Bothe, R. Brendel, Reduced module operating temperature and increased yield of modules with PERC instead of al-BSF solar cells, IEEE J. Photovolt. 7 (1) (2017) 44–50.

[10] B. Plesz, S. Ress, Investigation of the thermal behaviour of thin crystalline silicon solar cells, in: Thermal Investigations of ICs and Systems (THERMINIC), 2013 Proceedings of the 19th International Workshop on, IEEE, 2013, pp. 15–20.

[11] S. Sze, Wiley-Interscience Publication, John Wiley & Sons, 1981.

[12] J. Nelson, The Physics of Solar Cells, World Scientific Publishing Co Inc, 2003.

[13] J.C. Fan, Theoretical temperature dependence of solar cell parameters, Sol. Cells 17 (2) (1986) 309–315.

[14] J.J. Wysocki, P. Rappaport, Effect of temperature on photovoltaic solar energy conversion, J. Appl. Phys. 31 (3) (1960) 571–578.

[15] M.A. Green, General temperature dependence of solar cell performance and implications for device modelling, Prog. Photovolt. Res. Appl. 11 (5) (2003) 333–340.

[16] R. Couderc, M. Amara, M. Lemiti, In-depth analysis of heat generation in silicon solar cells, IEEE J. Photovolt. 6 (5) (2016) 1123–1131.

[17] A. Riverola, A. Mellor, D. Alonso Alvarez, L. Ferre Llin, I. Guarracino, C. Markides, D. Paul, D. Chemisana, N. Ekins-Daukes, Mid-infrared emissivity of crystalline silicon solar cells, Sol. Energy Mater. Sol. Cells 174 (2018) 607–615.

[18] B. Sopori, W. Chen, J. Madjdpour, N.M. Ravindra, Calculation of emissivity of Si wafers, J. Electron. Mater. 28 (12) (1999) 1385–1389.

[19] J. Brody, A. Rohatgi, V. Yelundur, Bulk resistivity optimization for low-bulk-life-time silicon solar cells, Progress. Photovolt.: Res. Appl. 9 (4) (2001) 273–285.

[20] S.C. Baker-Finch, K.R. McIntosh, D. Yan, K.C. Fong, T.C. Kho, Near-infrared free carrier absorption in heavily doped silicon, J. Appl. Phys. 116 (6) (2014) 063106.

[21] R. Couderc, M. Lemiti, M. Amara, Impact of the bias on the temperature of silicon solar cells under operating conditions, in: 2014 IEEE Proceedings of the 40th Photovoltaic Specialist Conference (PVSC), 2014-06, pp. 2463–2466.

[22] J. Haschke, J.P. Seif, Y. Riesen, A. Tomasi, J. Cattin, L. Tous, P. Choulat, M. Aleman, E. Cornagliotti, A. Uruena, R. Russell, F. Duerinckx, J. Champliaud, J. Levrat, A.A. Abdallah, B. Aïssa, N. Tabet, N. Wyrsch, M. Despeisse, J. Szlufcik, S. De Wolf, C. Ballif, The impact of silicon solar cell architecture and cell interconnection on energy yield in hot & sunny climates, Energy Environ. Sci. 10 (5) (2017) 1196–1206.